Development 139, 3432-3441 (2012) doi:10.1242/dev.080762

Atonal and EGFR signalling orchestrate *rok*- and *Drak*-dependent adherens junction remodelling during ommatidia morphogenesis

Francesca Robertson[1,2], Noelia Pinal[1,2], Pierre Fichelson[1,2] and Franck Pichaud[1,2,*]

SUMMARY

Morphogenesis of epithelial tissues relies on the interplay between cell division, differentiation and regulated changes in cell shape, intercalation and sorting. These processes are often studied individually in relatively simple epithelia that lack the complexity found during organogenesis when these processes might all coexist simultaneously. To address this issue, we are making use of the developing fly retinal neuroepithelium. Retinal morphogenesis relies on a coordinated sequence of interdependent morphogenetic events that includes apical cell constriction, localized alignment of groups of cells and ommatidia morphogenesis coupled to neurogenesis. Here, we use live imaging to document the sequence of adherens junction (AJ) remodelling events required to generate the fly ommatidium. In this context, we demonstrate that the kinases Rok and Drak function redundantly during Myosin II-dependent cell constriction, subsequent multicellular alignment and AJ remodelling. In addition, we show that early multicellular patterning characterized by cell alignment is promoted by the conserved transcription factor Atonal (Ato). Further ommatidium patterning requires the epidermal growth factor receptor (EGFR) signalling pathway, which transcriptionally governs *rok*- and *Drak*-dependent AJ remodelling while also promoting neurogenesis. In conclusion, our work reveals an important role for Drak in regulating AJ remodelling during retinal morphogenesis. It also sheds new light on the interplay between Ato, EGFR-dependent transcription and AJ remodelling in a system in which neurogenesis is coupled with cell shape changes and regulated steps of cell intercalation.

KEY WORDS: Adherens junction remodelling, Apical constriction, EGFR signalling, Bazooka, Myosin II, Drak, Rok, *Drosophila*

INTRODUCTION

During development, epithelial tissue remodelling requires regulated cell-cell junction rearrangements that are often polarized along the planar axis of the developing epithelium (Pilot and Lecuit, 2005; Zallen and Blankenship, 2008). In addition, many developing epithelia are patterned by the formation of a compartment boundary (Dahmann and Basler, 1999). These processes are conserved through evolution and together are likely to be broadly required during epithelial-derived organ morphogenesis (Bertet et al., 2004; Blankenship et al., 2006; Classen et al., 2005; Irvine and Wieschaus, 1994; Keller, 2002; Wallingford et al., 2000; Zallen and Wieschaus, 2004). The developing fly embryo has proven to be an excellent system with which to dissect the cellular and molecular machinery involved in the regulation of AJ dynamics and remodelling in various developmental contexts. These include apical cell constriction in the invaginating mesoderm (Sweeton et al., 1991), dorsal closure of the epidermis and planar polarized cell intercalation during germband extension, to name a but few examples (Irvine and Wieschaus, 1994). During germband extension in the fly embryo, AJs between antero/posterior (A/P) neighbours shrink, allowing adjacent dorso/ventral (D/V) cells to intercalate between A/P cells (Bertet et al., 2004; Zallen and Wieschaus, 2004). Both non muscle Myosin II (MyoII) and Bazooka (Baz) are required for this process (Zallen and Wieschaus, 2004; Bertet et al., 2004; Simoes Sde et al., 2010). In this tissue, the cellular pool of MyoII is found associated with a medial and cortical F-actin meshwork (Bertet et al., 2004; Fernandez-Gonzalez et al., 2009; Rauzi et al., 2008). Suppression of discrete AJs between A/P neighbours is driven by anisotropic, medial-to-cortical actomyosin contractile flows, and is facilitated by cortical MyoII at A/P contacts, which stabilizes the compaction of the junction (Rauzi et al., 2010). Within this epithelium, Baz adopts a localization complementary to MyoII and is found at stable D/V AJs (Blankenship et al., 2006). This complementary relationship has been documented in several other tissues, including the D/V and A/P boundaries of the developing wing and the denticle fields of the ventral epidermis (Landsberg et al., 2009; Major and Irvine, 2006; Simone and DiNardo, 2010). Interestingly, recent work has demonstrated that the *Drosophila* Rho-associated kinase (Rok) plays an instructive role in planar polarizing Baz and MyoII in intercalating cells in the germband (Simoes Sde et al., 2010). At A/P AJs, Rok is responsible for both the localization and activation of MyoII contractility, as well as exclusion of Baz from these contacts by phosphorylation of Baz at its C-terminal domain (Krahn et al., 2010; Simoes Sde et al., 2010).

It is clear that the core mechanisms and molecular players identified in simple epithelia will support many instances of epithelial remodelling and organogenesis in vivo. However, patterning of more complex epithelia, morphogenesis of which relies on orchestrated cell shape changes and AJ remodelling and also on the simultaneous differentiation of several cell types, is not well understood. The developing fly retina is a sensory neuroepithelium that provides us with a unique opportunity to tackle this issue. Retinal morphogenesis relies on the differentiation of many different

[1]MRC Laboratory for Molecular Cell Biology and Cell Biology Unit, University College London, Gower Street, London, WC1E 6BT, UK. [2]Research Department of Cell and Developmental Biology, University College London, Gower Street, London, WC1E 6BT, UK.

*Author for correspondence (f.pichaud@ucl.ac.uk)

Accepted 25 June 2012

cell types and is accompanied by a series of intricate cell shape changes that are generated simultaneously through apical cell constriction and discrete events of AJ remodelling that are also coupled to neurogenesis (Ready et al., 1976).

In *Drosophila*, patterning of the eye neuroepithelium arises from the morphogenetic furrow (MF), which travels along the A/P axis of the disc depositing regularly spaced clusters of photoreceptors called ommatidia. The MF is characterized by cells undergoing synchronous apical constriction and apicobasal contraction regulated downstream of Cubitus interruptus (Ci) (Corrigall et al., 2007; Escudero et al., 2007; Ready et al., 1976; Schlichting and Dahmann, 2008; Wolff and Ready, 1991). In this context, apical cell constriction depends on MyoII and the formin *diaphanous* (*dia*), but not RhoGEF2, WASP or dPak1 (Pak – FlyBase) (Corrigall et al., 2007; Escudero et al., 2007). Importantly, although *rok* acts upstream of MyoII during this process, our previous work and that of others indicate that another kinase must function redundantly (Corrigall et al., 2007; Escudero et al., 2007; Lee and Treisman, 2004). At the posterior margin of the MF, apically constricted cells rearrange themselves with respect to their neighbours and are organized into highly ordered, planar polarized multicellular structures. These structures represent the units that will develop into ommatidia (Wolff and Ready, 1991). The multicellular structures that emerge from the posterior margin of the MF are referred to as 'lines', 'arcs' and 'pre-clusters' (Escudero et al., 2007; Wolff and Ready, 1991) and eventually give rise to a highly ordered array of ommatidia in the eye disc.

MATERIALS AND METHODS

Genotypes used in this study

The following genotypes were used in this study: *yw;Ubi-ECad::GFP* (Oda and Tsukita, 2001); *hsflp122,Act>CD2>Gal4;UAS-m-YFP::myosinII DN* (Dawes-Hoang et al., 2005); *rok*^{2}*FRT19A/FRT19AUbiGFP;eyflp/+* (Winter et al., 2001); *w,baz*^{4}*FRT9.2/Ubi-GFPFRT9.2;eyflp/+* (Wodarz et al., 1999); *w,baz*$^{815\text{-}8}$*FRT 9.2/Ubi-GFPFRT9.2;eyflp/+* (McKim et al., 1996); Baz whole mutant eyes were generated by crossing *FRT19A,baz*^{GO484}*/Y;;UAS-Baz::GFP,Tub-Gal4/+* with *FRT19A,Minute,armlacZ/FM7;;eyflp/Tm6B,Tb* (Peter et al., 2002); *w,eyflp/+;;ato*^{1}*FRT82B/Ubi-GFPFRT82B* (Jarman et al., 1994); *w,eylflp,UASGFP;;FRT82B,ato*^{1}*/TubGal4,FRT82BTubGal80.-w,hsflp122;Tub>w[+]>Gal4/UAS-ato;eyflp/+;;pnt*$^{\Delta 88}$*FRT82/FRT82Minute,-armZ* (Scholz et al., 1993); *eyflp/+;;FRT80B ru*^{1}*,rho*^{7M43}*/FRT80AUbi-GFP* (Wasserman et al., 2000). Rok::Venus (Simoes Sde et al., 2010) was expressed in the developing eye. *rok*^{2}*,Drak*^{Del}*/Drak*^{ko} (Neubueser and Hipfner, 2010) and discs were examined for defects in constriction. *Drak*^{Del} (Neubueser and Hipfner, 2010) was recombined onto a *rok*^{2}FRT19A chromosome and recombinants were tested using PCR.

Fly cultures and crosses were carried out at 25°C and dissected 6-7 days after egg laying. Genotypes carrying an inducible *hsflp* to generate clones were raised for 4 days at 25°C prior to a 30-minute heat shock at 37°C. Crosses were then placed at 25°C for a further 3 days. Genotypes crossed with *w,hsflp122;Tub>w[+]>Gal4* and *hsflp122,Act>CD2>Gal4* were raised at 25°C for 4 days prior to a 30-minute heat shock at 37°C. Crosses were then placed at 29°C and dissected 48 hours later. The *rok*^{2}*,Drak*^{del} loss-of-function clones in the eye were induced at 18°C.

Immunostaining

Immunostaining was performed using the following primary antibodies: rat anti-ECadherin [1/50; Developmental Studies Hybridoma Bank (DSHB)]; mouse anti-Armadillo (1/50; DSHB); rabbit anti-PSer19-MRLC (1/10; Cell Signaling Technology, Beverly, MA, USA); rat anti-Bazooka (1/1000; A. Wodarz, Stem Cell Biology Unit, Göttingen, Germany); anti-dp-ERK (1/100; Sigma); rabbit anti-zipper (1/500; D. Kiehart, Duke University, Durham, NC, USA); rabbit anti-β-galactosidase (1/5000; Cappel Laboratories, Durham, NC, USA). Anti-mouse, anti-rabbit or anti-rat secondary antibodies were conjugated to either AlexaFluor 488, AlexaFluor 555, AlexaFluor 647, FITC, Texas Red or Cy5 (1/100; Jackson ImmunoResearch).

Imaginal discs were dissected in PBS and fixed in 4% formaldehyde for 20 minutes at room temperature. Antibodies were incubated in PBS containing Triton X-100 (0.3%). Imaging was performed using a Leica SP5 confocal microscope.

Live imaging

Live imaging was conducted on whole-mount pupae (Escudero et al., 2007). Prior to imaging, the cuticle over the head capsule was removed. The preparation was mounted such that the anterior region of the pupae lay elevated on a cushion of Blu-Tack, and the posterior region lay in contact with double-sided tape attached to the surface of a glass slide. A cover slip coated in voltalef oil was placed over the head, making contact specifically with the eye disc. Samples were imaged using an SP5 confocal microscope (Leica). An image was acquired every 1 μm in the *z* plane over a total of 20 μm to create a *z*-stack. This was carried out at four-minute intervals.

Quantification

Quantification was carried out using ImageJ (Abramoff et al., 2004) and Microsoft Excel Office. Quantification was carried out to compare the mutant tissue with wild-type (WT) tissue from the same disc. Mean pixel intensities were measured over a transect line though the corresponding junction and analysed using the 'RGB measure' plugin tool. Surface areas of WT and mutant patches of cells in the MF were also measured.

RESULTS

Ommatidia morphogenesis

As the MF travels towards the anterior pole of the eye disc, developing ommatidia are deposited in a regular array behind the MF (Fig. 1A,B). To document multicellular patterning during ommatidia morphogenesis, we analysed both fixed preparations and time-lapse recordings of discs in living pupae (Fig. 1C). The first instance of patterning that we can detect is the formation of lines that consist of five to seven cells (Fig. 1Ca′,D; supplementary material Movies 1, 2). These lines evolve into arcs, referred to here as type1-arcs, which contain a central core of four to five cells that are in contact with approximately nine to ten outer cells (Fig. 1Cc′). As the type1-arc evolves, the core cells are progressively excluded. Mature arcs, referred here as type2-arcs, present one central core cell that is in contact with six to seven outer cells (Fig. 1Ce′; supplementary material Movies 3, 4) that includes the presumptive R8 cell that at this stage has assumed a clear triangular shape (Wolff and Ready, 1991). In this cluster, the five central outer cells of the type2-arc are destined to become photoreceptors. In order to form a 5-cell pre-cluster, these cells must undergo a process of zipping up into a 'rosette configuration' (Fig. 1Ch′,D-F; supplementary material Movies 1-4 and Fig. S1A-E). Initially, the pre-clusters assume a rosette configuration that can transiently contain up to seven cells joined at a central vertex (Fig. 1Cg′). Over time, this structure resolves into a 6-cell rosette (Fig. 1Ch′). Subsequent AJ elongation from the central vertex results in the exclusion of one cell of indeterminate fate called a mystery cell (M1) (Wolff and Ready, 1991) to generate a typical 5-cell pre-cluster (Fig. 1Ci′). Together, these data largely corroborate previous work by Wolff and Ready (Wolff and Ready, 1991) using fixed preparations. Our work also reveals a new feature: the formation of a 6-cell rosette in which all cells share a central vertex, prior the formation of the classical 5-cell pre-cluster.

E-Cad and Baz share a complementary distribution to Rok and MyoII during retinal patterning

To characterize further the process of multicellular patterning during ommatidia morphogenesis, we next examined the expression pattern of E-Cad (Shg – FlyBase), Baz, MyoII and Rok. First, in the anterior compartment, Ser19P-MyoII is found both at

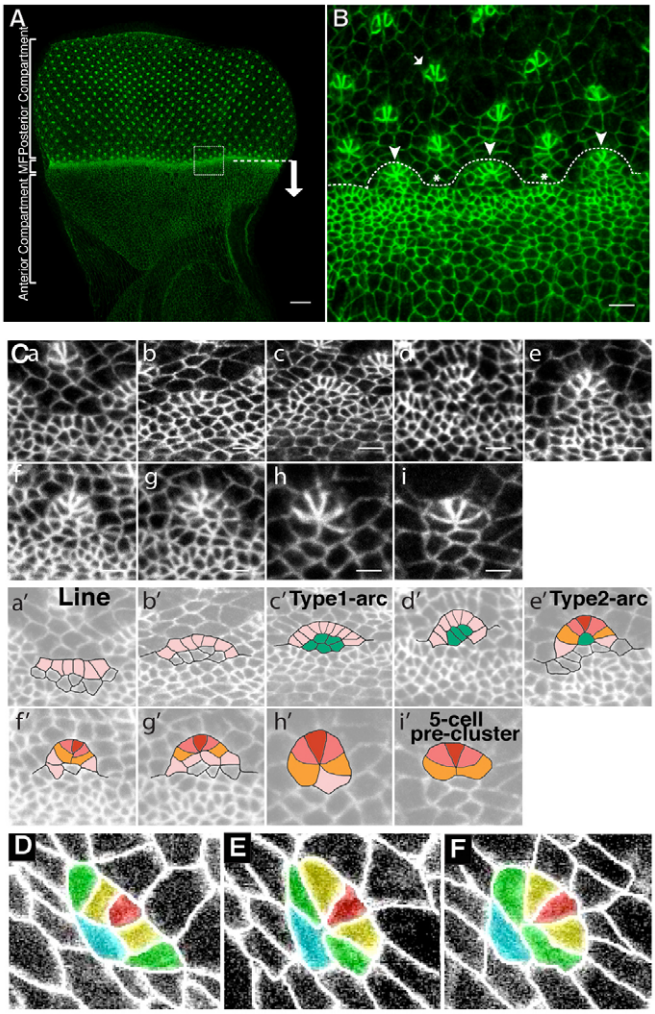

Fig. 1. Multicellular patterning in the developing *Drosophila* eye. (**A**) WT *Drosophila* eye imaginal disc. E-Cad::GFP (green). The MF is indicated by a dashed line. An arrow indicates the direction of MF movement. Scale bar: 20 μm. (**B**) Magnification of the boxed region in A. At the posterior margin of the MF, cells form patterned structures referred to as arcs and lines (indicated by the arrowheads and asterisks, respectively). These multicellular structures are then patterned into 5-cell pre-clusters (arrow). Scale bar: 4 μm. (**C**) Reconstruction of the sequence of events involved in ommatidium assembly (a-i). a, line; b-e, line-to-arc transition. Type1-arcs mature towards a Type2-arc configuration (e). g is a 7-cell rosette, which resolves into a typical 6-cell rosette (*n*=7 out of 7 ommatidia examined in independent retinas) (h) and then into a 5-cell pre-cluster (i). Scale bars: 3 μm. A schematic of these stages has been illustrated in Ca′-i′. Lines of cells (pink, a′) form the outer cells of the arcs, which reside adjacent to the core cells (green, c′). The R8 (red, e′) is adjacent to the R2/R5 precursors (dark pink, e′), and adjacent to those are the R3/R4 (orange, e′). These cells (R8, R2, R5, R3 and R4) form the 5-cell pre-cluster (i′). (**D-F**) Stills from a time-lapse movie (supplementary material Movies 1, 3) of whole-mount pupae ubiquitously expressing E-Cad::GFP depicting a line of five cells (D), a 6-cell rosette configuration (E) and a 5-cell pre-cluster (F). Red is R8, the presumptive R2/R5 are yellow, the presumptive R3/R4 are green and the Mystery cell 1 is in turquoise (Wolff and Ready, 1976).

discrete foci associated with the cells' zonula adherens (ZA) and also as a medial meshwork (Fig. 2A). This distribution is consistent with the observation that these cells are in the process of constricting (Corrigall et al., 2007; Martin et al., 2009). In addition, we note that when Ser19P-MyoII localizes at the cortex, this is correlated with a reduction in the level of ZA-associated Baz (Fig. 2A-C). In the MF (Fig. 2D-F), the association of Ser19P-MyoII with the ZA of constricted cells is more prominent (Fig. 2D). Strong foci of Ser19P-MyoII correlate with a reduction in the level of Baz (Fig. 2D-G). This demonstrates that at the ZA, Baz and Ser19P-MyoII present a segregated pattern of localization in the cells of the anterior compartment. In the MF, when cell constriction reaches a maximal level, the segregated localization of Baz and Ser19P-MyoII at the cell ZA is greatly exacerbated.

Next, we examined the lines and arcs emerging from the MF. We observe that Ser19P-MyoII becomes enriched in the posterior AJs of aligned groups of cells (Fig. 2H-K). Interestingly, we also find that a kinase-dead fusion protein of Rok is enriched in the posterior AJs (supplementary material Fig. S2G-I). As the line develops into a type1-arc, posterior AJs in the outer cells of the arcs remain enriched with Ser19P-MyoII and Rok (Fig. 2L-N). In both lines and arcs, E-Cad and Baz are also planar polarized, and are enriched in the mediolateral AJ that are orthogonal to the posterior AJs (Fig. 2J,M; supplementary material Fig. S2A-F). Quantification of the length of the posterior AJs demonstrates that they are significantly shorter than the mediolateral AJs in both lines and arcs (supplementary material Table S1). This is consistent with MyoII exerting a contractile force onto the posterior AJs. When quantified, the level of Baz at posterior AJs in lines and arcs was approximately half of that measured in mediolateral junctions (Fig. 2J,M,O,P; supplementary material Table S2). Similarly, E-Cad levels at the posterior AJs were ~60% of those measured at the mediolateral AJ in lines and arcs (supplementary material Fig. S2A-F and Table S2). Similarly, E-Cad levels at the posterior AJs were ~0.78 and 0.65 times that of mediolateral AJ in lines and arcs, respectively (supplementary material Fig. S2A-F and Table S2). Furthermore, quantification of pixel intensity reveals that Ser19P-MyoII is ~2 and 2.5 times more enriched in these posterior AJs relative to the mediolateral AJs within lines and arcs, respectively (Fig. 2O,P; supplementary material Table S2). Finally, examining the transition from type2-arcs to 6-cell rosettes indicates that high levels of Ser19P-MyoII are associated with two contiguous AJs that will be suppressed during this process (Fig. 2Q and Fig. 1Cf′-Ch′). This is compatible with MyoII promoting selective suppression of AJs. In the rosette, Ser19P-MyoII remains distributed all around the cell cluster, but is also concentrated at the common AJ vertex at the centre of the rosette (Fig. 2R). This suggests that the common vertex configuration is actively maintained.

rok promotes AJ remodelling during ommatidia morphogenesis

MyoII is required to generate cell constriction in the MF (Fig. 3A-D). In addition, lines and arcs are completely lost when expressing the dominant-negative version of the MyoII heavy chain, *mYFP-MyoII*^{DN} (Fig. 3A-D). In this condition, Baz and Arm remain expressed non-uniformly around the corresponding cell-cell contacts (Fig. 3B′,C′). This is consistent with expression of this transgene not completely abolishing MyoII activity, as medio-cortical filaments of MyoII can still be detected in this condition (supplementary material Fig. S2J-M). Nevertheless, from these observations, we conclude that in the posterior AJs, regulated MyoII localization and activation is required to promote the planar polarization of Baz and E-Cad in the mediolateral AJs.

Although Rok promotes cell constriction in the MF, it is clear that another kinase must act redundantly during this process as *rok*^{2} mutant clones only partially abolish apical cell constriction in the

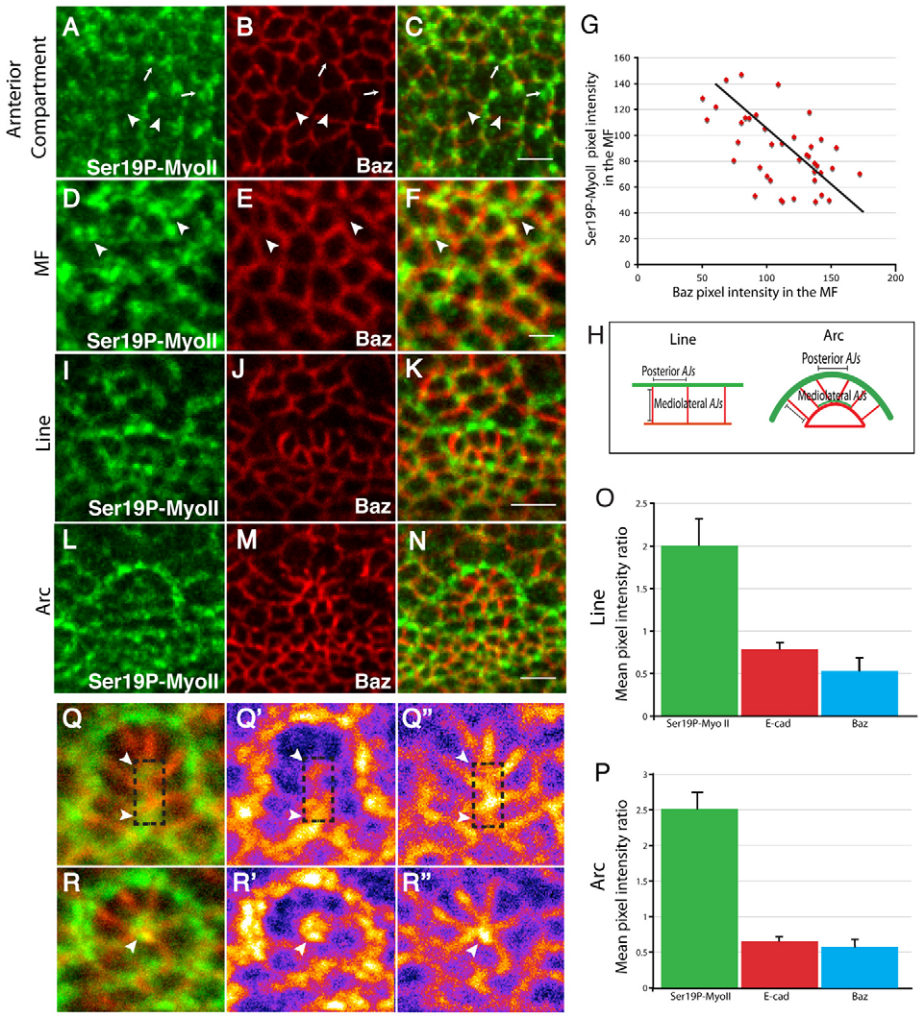

Fig. 2. E-Cad, Baz and MyoII are planar polarized during ommatidia patterning. (**A-C**) Anterior compartment of a WT *Drosophila* eye disc stained for SerP19-MyoII (green) and Baz (red). Strong foci of Ser19P-MyoII at the ZA correspond with a reduction in Baz levels at the ZA (arrows). Arrowheads point to medial meshwork of MyoII. Scale bar: 4 μm. (**D-F**) MF of a WT eye disc stained for SerP19-MyoII (green) and Baz (red). Strong foci of Ser19P-MyoII correspond with a reduction in Baz levels at the ZA (arrowheads). Scale bar: 1 μm. (**G**) Quantification of the pixel intensity of Ser19P-MyoII and that of Baz at the ZA of MF cells. Each data point reflects a single pixel, measured randomly at the level of ZA across MF. (**H**) A schematic of a line and an arc. MyoII (green) is planar polarized in the posterior AJs of the lines and arcs, whereas E-Cad and Baz (red) are enriched in orthogonal, mediolateral AJs. (**I-N**) Ser19P-MyoII (green) and Baz (red) staining reveal a typical line (I-K) and a typical arc (L-N). Scale bars: 2 μm. (**O**,**P**) Quantification of the level of E-cad (red), SerP19MyoII (green) and Baz (blue) in posterior AJs versus mediolateral AJs, in lines (O) or arcs (P). For each protein, the average pixel intensity of all posterior AJs per ommatidium was compared with the average pixel intensity of all mediolateral AJs per ommatidium. Error bars indicate the s.d. between ommatidia. (**Q-Q″**) Representative transition phase from a type2-arc towards a 6-cell rosette (number of transitions monitored=9). SerP19-MyoII (green), Baz (red). MyoII is enriched at the AJs that are undergoing suppression (boxed area). White arrowheads point to AJs that are associated with SerP19-MyoII and that show a relative depletion of Baz (red). Images in Q′and Q″ were created using the Fire filter from FIJI. (**R-R″**) Representative 6-cell rosette in the process of becoming a 5-cell pre-cluster (number of transitions monitored=7). SerP19-MyoII (green), Baz (red). SerP19-MyoII is strongly associated with the central vertex of the rosette (white arrowhead). Images in R′ and R″ were created using the Fire filter from FIJI.

MF (Corrigall et al., 2007; Escudero et al., 2007; Lee and Treisman, 2004) (Fig. 3E-H; supplementary material Fig. S2N-Q). In *rok*^{2} mutant clones, Baz and Arm segregate normally to mediolateral AJs in the wake of the MF (Fig. 3E-H; supplementary material Fig. S2R-U). However, we note a clear role for this kinase during the development of type2-arcs into 6-cell rosettes (Fig. 1Ce′-Ci′ and Fig. 3E-H) as *rok*^{2} mutant clusters fail to assemble a central vertex between ommatidial precursor cells (Fig. 3H1,H2; phenotype penetrance=100% in 11 clusters examined). The supernumerous AJs detected in the absence of *rok*^{2} function (Fig. 3H1‴,H2‴) correspond to those normally associated with Ser19P-MyoII (Fig. 2Q-Q″). This suggests that in the absence of *rok* function, the failure to eliminate AJs during ommatidium morphogenesis might be due to a failure to properly activate MyoII at these AJs.

Drak and Rok function redundantly during multicellular patterning

Recent work has demonstrated that the Death-associated protein kinase (Drak) can act redundantly with Rok during development

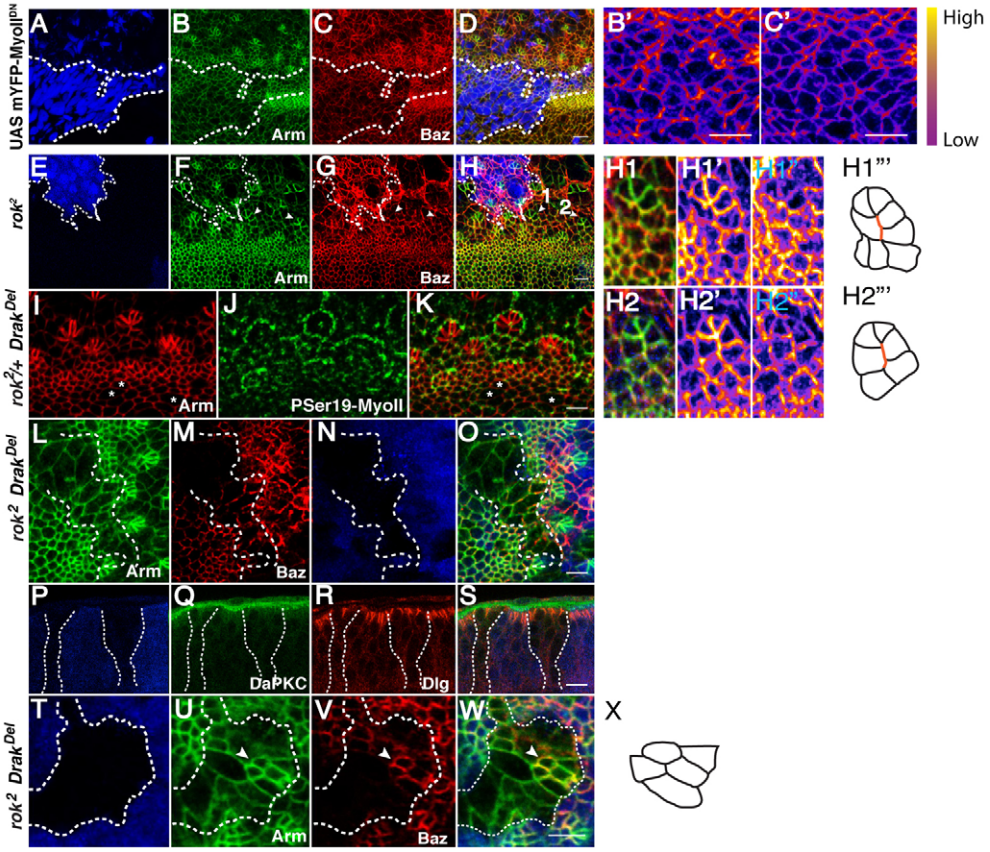

Fig. 3. *rok* and *Drak* are required for MyoII-dependent multicellular patterning in *Drosophila*. (**A-D**) Clones expressing the mYFP-MyoII^{DN} transgene (blue) also stained for Arm (green) and Baz (red). B′ and C′ show a high magnification of the area expressing the mYFP-MyoII^{DN} transgene in A-D. The fire filter from FIJI is used to reveal the regions of high concentration versus low concentration of Baz (B′) and Arm (C′) at the cell's ZA. (**E-H2‴**) *rok*^{2} clones are indicated by the absence of GFP (in blue). Green, Arm; red, Baz. White arrowheads point to abnormally configured ommatidial clusters (1 and 2) that are magnified in H1-H1‴ and H2-H2‴. H1′ and H2′ show the Arm channel and H1″ and H2″ show the Baz channel. The supernumerous AJs that should have been suppressed in order to accommodate the transition between type2-arc and 6-cell rosette are annotated with a red line in H1‴ and H2‴. (**I-K**) *rok*^{2}/+, *Drak*^{Del} whole mutant eyes stained for Arm (red) and SerP19MyoII (green). *rok*^{2}/+ *Drak*^{Del} mutant eyes display local instances of impaired constriction (indicated by asterisks). (**L-O**) *rok*^{2}, *Drak*^{Del} clones lack GFP (blue). Green, Arm; red, Baz. (**P-S**) Sagittal section of clones mutant for *rok*^{2}, *Drak*^{Del} (lacking blue). Green, DaPKC; red, Dlg. (**T-W**) *rok*^{2}, *Drak*^{Del} clone lacking GFP (blue). Green, Arm; red, Baz. Arrowheads indicate a developing ommatidium. (**X**) Cluster observed in the absence of *rok* and *Drak* function. Scale bars: 5 μm. Dashed lines outline the mutant tissue.

(Neubueser and Hipfner, 2010). Examination of retina lacking Drak function and heterozygous for *rok*^{2} revealed instances of impaired cell constriction (Fig. 3I-K). We next induced *Drak*^{Del} *rok*^{2} mutant clones in the eye. In these clones, apicobasal epithelial polarity is retained (Fig. 3L,P-S). Although these mutant cells remain largely columnar (Fig. 3P-S), apical constriction is completely abolished (Fig. 3L-O). In addition, the loss of both *Drak* and *rok* prevents the further steps of AJ remodelling from proceeding normally during ommatidia morphogenesis (Fig. 3T-X). From this, we conclude that Drak and Rok function redundantly throughout ommatidia morphogenesis.

Baz promotes AJ remodelling during ommatidia morphogenesis

We next tested Baz function during AJ remodelling in the developing ommatidium. In loss-of-function clones for the strong hypomorphic allele *baz*^{4} and the null allele *baz*$^{815-8}$, most of the posterior AJs in lines and arcs remain enriched with Ser19P-MyoII (Fig. 4A-G) (data not shown). In addition, E-Cad remains enriched in the mediolateral AJs. We note, however, discrete instances of Ser19P-MyoII localization at mediolateral AJs (1.5 AJ per type1-arc on average; *n*=10 arcs), suggesting that Baz contributes to limiting MyoII localization to the posterior AJs (Fig. 4E-G). In addition, close inspection of *baz*^{4}, *baz*$^{815-8}$ and *baz*^{GO484} mutant clones revealed consistent irregularities in the configuration of cell contacts within the developing pre-clusters (Fig. 4H-K). Specifically, within WT type2-arcs (Fig. 1Ce′), the differentiating R8 cell typically assumes a triangular 'V' shape, separating the presumptive R2/R5 precursors (100% of type2-arcs examined; *n*=17). However, in *baz* mutant eyes, the AJs separating these neighbours take on a 'Y' conformation that allows the cells on either side of the R8 to contact one another (Fig. 4L-M′). Consequently, the corresponding type2-arcs fail to assemble a central vertex and the 'Y' conformation persists, causing the ommatidium to elongate into a 'string of paired cells' (100% of type2-arcs examined; *n*=9). This phenotype is identical to that observed in the absence of *rok*^{2} function (Fig. 3H1‴,H2‴), suggesting that it might be linked to a function for Baz in

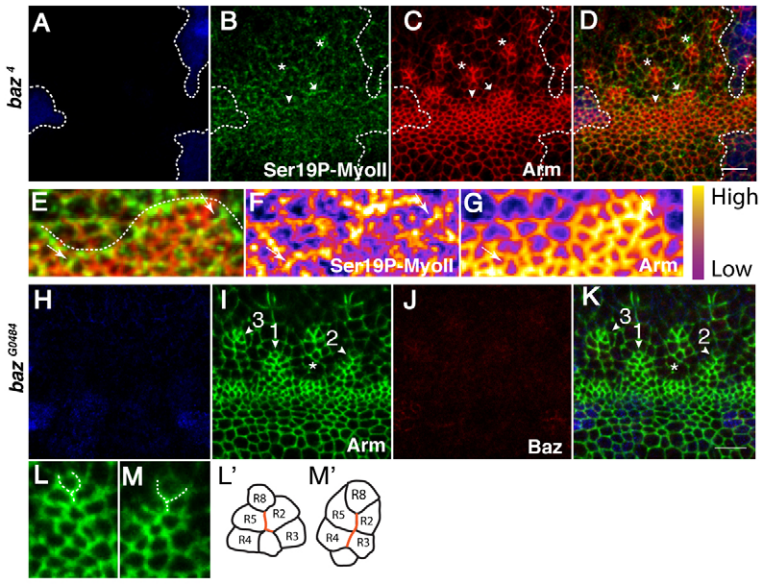

Fig. 4. *baz* is required for AJ remodelling during ommatidia morphogenesis in *Drosophila*. (**A-D**) *baz*^{4} clone lacking GFP (blue). Green, Ser19P-MyoII; red, Arm. The arrowhead points to a line and the arrow points to an arc. Asterisks indicate type2 arcs having failed to generate 6-cell rosettes. Dashed lines outline the mutant tissue. (**E-G**) Higher magnification of the line and arc shown in A-D. A dotted line highlights the supra-cellular cable of MyoII at the posterior AJs. Ser19P-MyoII (F) and Arm (G). White arrows point to ectopic Ser19P-MyoII invading the mediolateral AJs. (**H-K**) Whole eyes mutant for *baz*^{GO484}, lacking *lacZ* (indicated by β-galactosidase, blue). Green, Arm; red, Baz. Mutant clusters are denoted by the arrowheads 1-3. AJs separating R2 and R5 from the R8 take on a 'Y' conformation (arrowhead 1). More mature arcs elongate into a 'string of paired cells' (arrowhead 2). This defect leads to the loss of the common vertex normally shared between the R2, R8, and R5 precursors (arrowhead 3). A white asterisk marks a line emerging from the MF. (**L**,**M**) Higher magnification of ommatidia clusters 1 and 2, respectively. A dashed line highlights the 'Y' conformation found between the R8 and R2/5 neurons (**L′**,**M′**) Schematic of clusters 1 and 2, respectively. AJs that have failed to be suppressed during the transition from a type2-arc towards the 6-cell rosette configuration are depicted in red. Scale bars: 5 μm.

promoting localized MyoII activity, thus driving AJ suppression. Interestingly, we note that more mature ommatidia appear to eventually recover their normal configuration (i.e. 5-cell pre-clusters), suggesting that in addition to this function for Baz, redundant mechanisms regulating AJ remodelling must exist during ommatidia morphogenesis. Nonetheless, from these data we conclude that Baz promotes the coalescence of AJs into a central vertex to produce a 6-cell rosette.

Ato is required for planar polarization of E-Cad, Baz and MyoII, and the establishment of the MF posterior boundary

An important question is which upstream regulators are responsible for orchestrating the necessary steps of AJ remodelling during multicellular patterning in the developing retina? Ato is a basic helix-loop-helix transcription factor that is necessary for cell fate specification (Jarman et al., 1994) and multicellular patterning in the eye (Brown et al., 2006). We therefore sought to test its role in promoting E-Cad, Baz and MyoII planar polarization during ommatidia morphogenesis. In clones of cells mutant for *ato*^{1}, the cells in the MF appear slightly less constricted than in the WT (Fig. 5E-G; supplementary material Table S3). In addition, Baz and MyoII are no longer localized in recognizable mediolateral and posterior AJs, respectively (Fig. 5A-D). However, Baz and Ser19P-MyoII still present a segregated pattern of expression at the mutant cells' ZA (Fig. 5B′-D′). We note that E-Cad enrichment in the mediolateral AJs is also lost at the posterior margin of the MF (Fig. 5E-G). However, as is the case for Baz, E-Cad expression still appears to be non-uniform at the cells' ZA (Fig. 5H,I). Ato is, therefore, crucial for directing planar polarized Baz and MyoII to the mediolateral and posterior AJs, respectively. Interestingly, in *ato*^{1} mutant clones there appears to be a reduction in the level of ZA-associated E-Cad in MF cells in comparison with the neighbouring WT tissue (Fig. 5E-G; supplementary material Table S4). This is consistent with Ato promoting E-Cad transcription (Brown et al., 2006).

Next, we wanted to test whether ectopic expression of *ato* was sufficient to promote cell alignment in epithelia. When induced in the anterior compartment of the eye disc, ectopic *ato* clones display cells that are constricted and have elevated Baz and E-Cad levels (Fig. 5L,P; supplementary material Tables S5, S6). Importantly, Ser19P-MyoII accumulates at the interface between *ato*-expressing and non-*ato*-expressing cells (Fig. 5J-N). Along this multicellular MyoII cable, cells both within and outside the clone align along the length of the clone's boundary (Fig. 5N). Interestingly, Ser19P-MyoII accumulation at the clonal boundary also correlates with a reduction in the level of Baz at these AJs compared with those within the clone (Fig. 5L,N). These data indicate that generating an interface between *ato*-expressing and non-*ato*-expressing (*ato*+/*ato*–) cells is sufficient to induce the planar polarized accumulation of activated MyoII along this interface. Moreover, the multicellular polarization of MyoII along the *ato*+/*ato*– interface is accompanied by cell alignment. This is reminiscent of the situation found at the posterior boundary of the MF, and suggests that the restricted expression of Ato at the posterior margin of the MF drives the accumulation of Rok and MyoII at the posterior AJs together with limiting that of Baz and E-Cad to the mediolateral AJs.

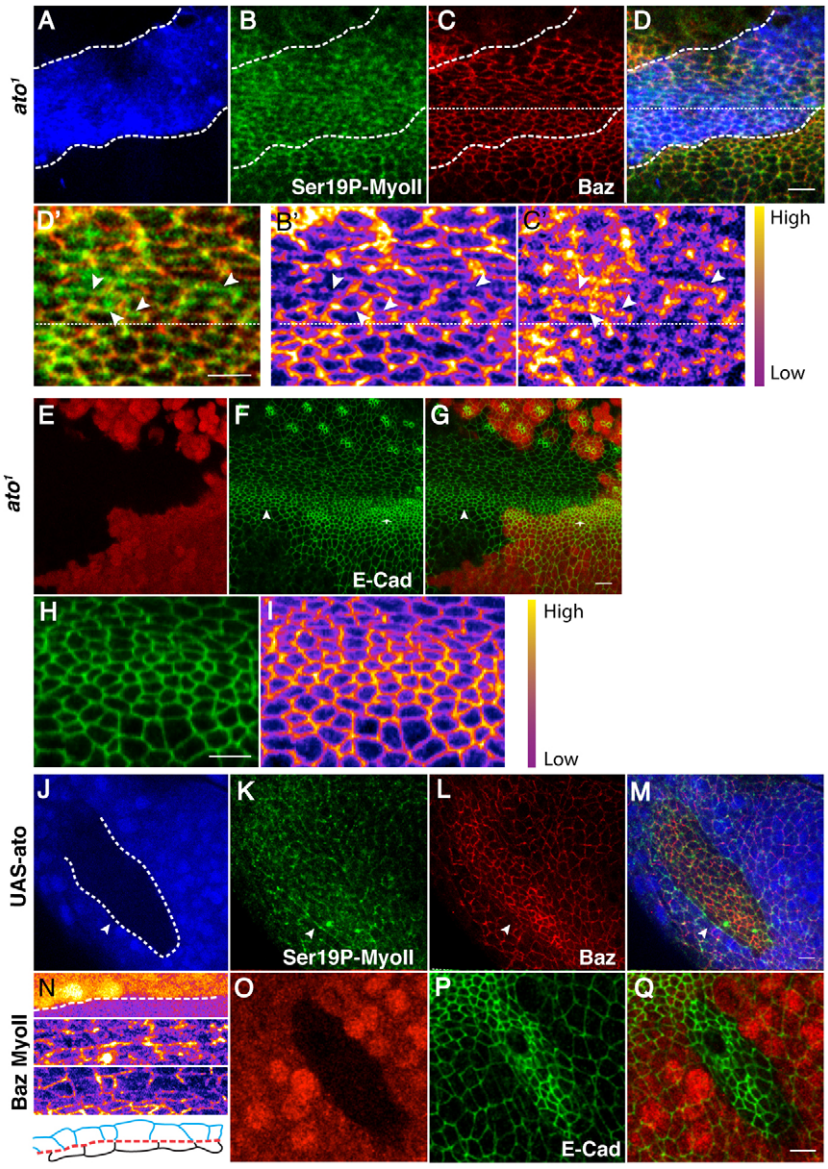

Fig. 5. Ato is required to set up the posterior and mediolateral AJs in the wake of the MF in *Drosophila*. (**A-D'**) *ato*^{1} clone lacking GFP (blue). Green, Ser19P-MyoII; red, Baz. The dashed lines indicate the position of the MF. Dotted lines delineate the mutant tissue. (B′-D′) Higher magnification of the *ato*^{1} mutant clone shown in A-D. D′ shows Ser19P-MyoII (green) and Baz (red); B′ shows Baz channel; C′ shows Ser19P-MyoII channel. Arrowheads point to examples of AJs that are rich in Ser19P-MyoII and depleted for Baz. (**E-G**) *ato*^{1} mutant cells (arrowhead) lack GFP (red). Green, E-Cad. The WT MF is indicated by the arrow. (**H**,**I**) Higher magnification of the *ato*^{1} mutant clone shown in E-G. (**J-M**) Clones ectopically expressing *UAS-ato* in the anterior compartment of the eye disc lack GFP (blue). A dashed line marks the *ato+/ato-* interface. (**N**) Close up and schematic of the interface between the Ato+ and Ato– cells as seen in J-M and marked by the white arrowhead. From top to bottom: top panel is the GFP channel where the *ato+/ato-* interface is highlighted by the dashed line. The next panel shows Ser19P-MyoII, followed by Baz. The last panel is a drawing of the corresponding cells with WT cells (*ato–*) in blue, the MyoII cable in red and Ato+ cells in black. (**O-Q**) Clones ectopically expressing a *UAS-ato* transgene in the eye disc lack GFP (red). Green, E-Cad. Scale bars: 5 μm.

EGFR governs AJ remodelling during ommatidia maturation

ato is required to promote EGFR signalling in the MF (Chen and Chien, 1999), and has been demonstrated to do so by upregulating the protease Rhomboid-1 (Rho) (Baonza et al., 2001). EGFR signalling has also been shown to be required for ommatidia patterning (Brown et al., 2006). We therefore investigated what role EGFR signalling plays in promoting Baz and MyoII localization and activity during AJ remodelling. To this end, we generated whole mutant eyes for the Ets transcription factor Pointed (Pnt) (O'Neill et al., 1994), which abolishes transcriptional output downstream of EGFR. In this context, multicellular alignment is still observed at the posterior margin of the MF (Fig. 6A-H). Likewise, within these lines, Baz and Arm are planar polarized and localize preferentially at the mediolateral AJs (Fig. 6F). Similarly, EGFR mutant eye discs show a clear F-actin-rich cable delineating the posterior boundary of the MF (not shown), indicating that EGFR signalling is not required for initiation of cell alignment. However, whole eyes mutant for *pnt*$^{\Delta 88}$ display defects in arc formation. We observe 'proto-arcs' in the MF, which represent an early step towards patterning a type1-arc (Fig. 6A-G). Our data are therefore consistent with transcription downstream of EGFR being required for proper AJ remodelling to form type1-arcs. In order to determine whether this function for EGFR is ligand dependent, we next examined multicellular pattern formation in double *rho,ru* loss of function, a genotype that leads to a failure to process EGFR ligands (Wasserman et al., 2000). In large *rho,ru* mutant clones, planar polarization of MyoII and Baz appears to be largely unaffected at the posterior and mediolateral AJs, respectively, both in lines and in structures that resemble proto-arcs (Fig. 6I-L). This phenotype is identical to that observed in the absence of *pnt* function, indicating that ligand-dependent EGFR signalling is required for the transition from a line into a type1-arc. This function for the EGFR signalling pathway correlates with the observation that, as previously demonstrated using anti-double phosphorylated extracellular-signal-regulated kinase (dp-ERK) (Rl – FlyBase) staining (Brown et al., 2006), the mitogen-activated protein kinase (MAPK) pathway is activated in the cells that are found in the lines and type1-arcs located the wake of the MF (Fig. 6M-P).

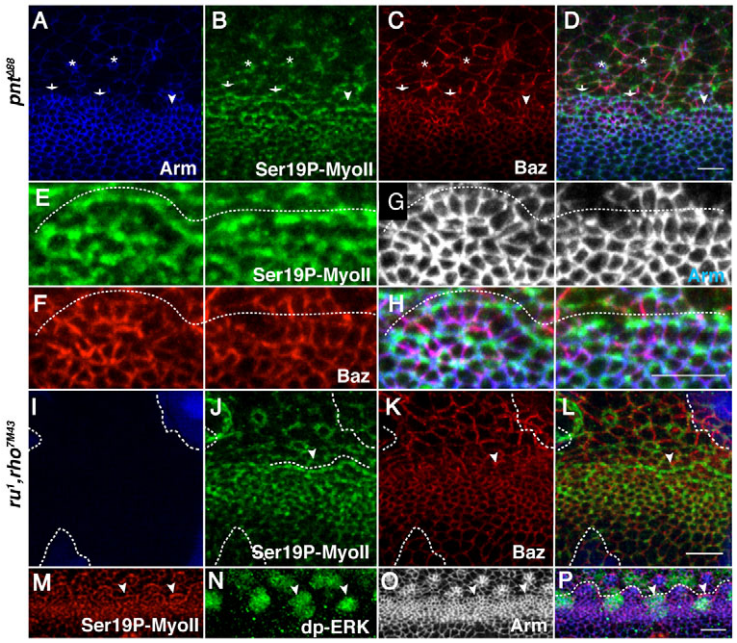

Fig. 6. Ligand-dependent EGFR signalling orchestrates AJ remodelling during ommatidia patterning in *Drosophila*. (**A-D**) Whole eyes mutant for $pnt^{\Delta 88}$. Green, Ser19P-MyoII; red, Baz; blue, Arm. 'Proto-arcs' are denoted by the arrows. Ser19P-MyoII, Baz and Arm retain their WT polarization in lines (arrowheads) and 'proto-arcs' (arrows) in the MF. Two representative R8 cells are denoted by asterisks. (**E-H**) Higher magnification of the line and proto-arc depicted in A-D. Ser19P-MyoII (E), Baz (F), Arm (G), merge (H). A dashed line delineates the supra-cellular cable of Ser19P-MyoII. (**I-L**) *rho,ru* clones lack GFP (blue). Green, Ser19P-MyoII; red, Baz. The posterior boundary of the MF is denoted by a dashed line. Lines are denoted by the arrowhead. (**M-P**) WT MF stained for dp-ERK (MAPK; green), Ser19P-MyoII (red) and Arm (grey). Arm is in blue in P. White arrowheads point to lines. A dashed line delineates the posterior boundary of the MF (lines and arcs). Scale bars: 5 μm.

DISCUSSION

Epithelial cell constriction and multicellular pattern formation

In *Drosophila*, Rok seems to be the main kinase responsible for phosphorylating the Myosin regulatory light chain (Sqh) during epithelial patterning and apical cell constriction (Quintin et al., 2008). This is the case for the activation of MyoII during intercalation as germband extension proceeds (Bertet et al., 2004; Simoes Sde et al., 2010), but also during various instances of compartment boundary formation and cell sorting situations in the embryo (Monier et al., 2010) and in the wing imaginal disc (Landsberg et al., 2009). Our work reveals that in the constricting cells of the MF, Rok functions redundantly with Drak, a kinase recently shown to phosphorylate Sqh both in vitro and in vivo (Neubueser and Hipfner, 2010). It is noteworthy that previous work has shown that *RhoGEF2* is not required for cell constriction in the MF (Corrigall et al., 2007; Escudero et al., 2007), suggesting that perhaps another guanine exchange factor (GEF) might function redundantly with RhoGEF2 to promote cell constriction. Our data on *Drak* reinforce the idea that redundancies exist in this context. Because the *RhoA* (*Rho1* – FlyBase) loss of function abolishes this cell response entirely (Corrigall et al., 2007), we would expect Drak function to be regulated by RhoA. In addition, our data indicate that Drak acts redundantly with Rok during MyoII-dependent multicellular alignment and AJ remodelling during ommatidia patterning. It will be interesting to test whether Drak functions in other instances of epithelial cell constriction or MyoII-dependent steps of AJ remodelling in other developmental contexts in *Drosophila*.

Compartment boundary and cell intercalation during retina morphogenesis

We demonstrate a two-tiered mechanism regulating the planar polarization of MyoII and Baz. In the constricting cells in the posterior compartment, MyoII and Baz are segregated from one another and this is exacerbated by the wave of cell constriction in the MF. Upon Ato-dependent transcription in the MF cells, this segregated pattern of expression is harnessed and these factors become planar polarized at the posterior margin of the MF. This is independent of the core planar polarity pathway including the Fz receptor (data not shown) and is accompanied by a striking step of multicellular alignment. Previous work has demonstrated that Ato upregulates E-Cad transcription at the posterior boundary of the MF (Brown et al., 2006). In addition, apical constriction leads to an increase in E-Cad density at the ZA. Our data are therefore consistent with both *hh*-dependent constriction (Corrigall et al., 2007; Escudero et al., 2007; Schlichting and Dahmann, 2008) and *ato*-dependent transcriptional upregulation of E-Cad promoting differential adhesion (Steinberg, 2007), thus leading to a situation in which the *ato*+ cells maximize AJ contacts between themselves and minimize contact with the flanking cells that express much less E-Cad at their ZA (Fig. 7). This typically leads to a preferential accumulation of cortical MyoII at the corresponding interface. Such actomyosin cables are correlated with increased interfacial tension (Landsberg et al., 2009; Monier et al., 2010) and we propose that this is in turn responsible for promoting cell alignment. Unfortunately, the very small diameter of these constricted cells precludes direct measurements of the AJ-associated tension using laser ablation experiments (F.R. and F.P., unpublished data).

Supra-cellular cables of MyoII have been previously associated with cell alignment in various epithelia (Nishimura et al., 2007; Simone and DiNardo, 2010; Walters et al., 2006) and have also been observed at the boundary of sorted clones, whereby cells align at a MyoII-enriched interface (Chang et al., 2011; Le Borgne et al., 2002; Wei et al., 2005). Interestingly, we find that the actomyosin cable defining the posterior boundary of the MF is also preferentially enriched for Rok, a component of the T1, MyoII-positive AJ in the ventral epidermis (Simoes Sde et al., 2010). This indicates an important commonality between actomyosin cable formation during cell sorting and the process of cell intercalation. However, unlike during intercalation, we found that in the developing retina *baz* is largely dispensable for directing the pattern of E-Cad and actomyosin planar polarization. Further work will therefore be required to understand better the relationship between Baz and E-Cad at the ZA during ommatidia morphogenesis. We

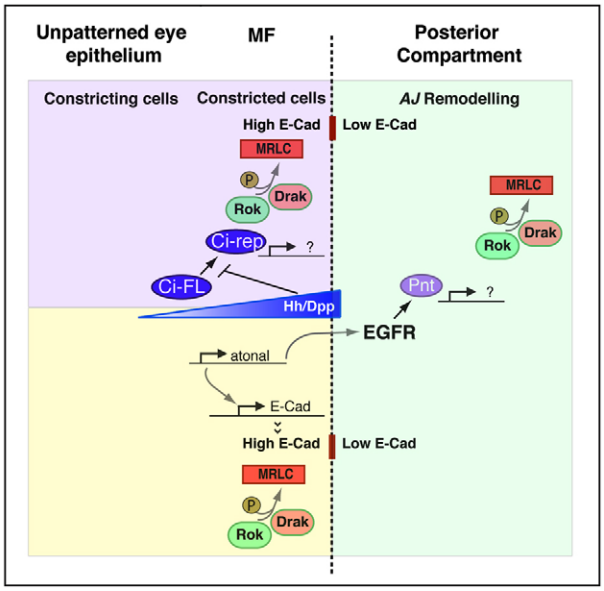

Fig. 7. Coordinated function of Hh, Ato and EGFR signalling during ommatidia patterning. Genetic network involved in promoting neuroepithelial patterning in the developing fly retina. Hh and Dpp signalling transcriptionally promote apical cell constriction via Ci (Corrigall et al., 2007; Escudero et al., 2007; Schlichting and Dahmann, 2008). *rok* and *Drak* function redundantly during cell constriction by phosphorylating Myosin Regulatory Light Chain (MRLC; Sqh – FlyBase). Transcription of *atonal* is activated downstream of Hh/Dpp and this factor in turn upregulates E-Cad transcription at the posterior boundary of the MF (Brown et al., 2006). As a consequence of both cell constriction and E-Cad upregulation, cells in the MF present higher levels of E-Cad compared with their neighbours in the posterior compartment. We hypothesize that this leads to differential adhesion, a process that causes the accumulation of an acto-myosin cable at the interface (indicated by a dashed line) between high and low levels of ZA-associated E-Cad (Steinberg, 2007). In the posterior compartment (green) EGFR functions downstream of *atonal* during multicellular patterning in the eye (Brown et al., 2006) and transcriptionally promotes (via Pointed, Pnt) discrete steps of AJ remodelling that require both *rok* and *Drak* function.

speculate that the creation of a high E-Cad versus low E-Cad boundary in the wake of the MF might be sufficient to promote Rok and MyoII enrichment at the posterior AJs. This posterior Rok and MyoII enrichment might perhaps prevent E-Cad accumulation by promoting E-Cad endocytosis, as has been recently shown in the fly embryo (Levayer et al., 2011).

AJ remodelling during ommatidia morphogenesis

We have used live imaging to define a conserved step of ommatidia patterning that consists of the coalescence of the ommatidial cells' AJs into a central vertex to form a 6-cell rosette. We find that the corresponding steps of AJ remodelling require Rok, Drak, Baz and MyoII, a situation compatible with mechanisms previously identified during cell intercalation in the developing fly embryo. We also show that the steps of AJ remodelling required to transform lines of cells into 5-cell pre-clusters are transcriptionally regulated downstream of EGFR in a ligand-dependent manner. Interestingly, we and others (Brown et al., 2006) find that in the eye, EGFR signalling is activated in the cells that form lines and type1-arcs in the wake of the MF and, thus, are undergoing AJ remodelling. Previous work examining tracheal morphogenesis in the fly has demonstrated that interfaces between cells with low levels versus high levels of EGFR signalling correlate with MyoII-dependent AJ remodelling in the tracheal placode (Nishimura et al., 2007). This situation resembles that which we describe here in the wake of the MF. In the eye, however, we find that EGFR signalling is not required to initiate cell alignment. Nevertheless, taken together with work in the tracheal placode and previous studies related to multicellular patterning in the developing eye (Brown et al., 2006; Escudero et al., 2007), our work indicates a conserved function for the EGFR signalling pathway in promoting MyoII-dependent AJ remodelling. This leaves open several interesting questions; for example, it is not presently clear how EGFR signalling can promote discrete AJ suppression and elongation. It is, however, tempting to speculate that previously described links between EGFR signalling and the expression of E-Cad (Brown et al., 2006; O'Keefe et al., 2009) or Rho1 (Brodu and Casanova, 2006) might play a role during this process.

Acknowledgements

The authors would like to thank Matthew Freeman, David Hipfner, Jessica Treisman, Andreas Wodarz and Jennifer Zallen for kindly providing us with fly stocks and reagents; the Bloomington Stock Center for fly stocks; and the Developmental Studies Hybridoma Bank for antibodies. We are grateful to Rhian Walther for her help with preparing the manuscript and to Elisa Salamanca for her help with dissections and fly crosses.

Funding

F.R. is a recipient of a Medical Research Council (MRC) PhD scholarship. N.P. and P.F. were supported by an MRC Career Development Fellowship. Work in F.P.'s laboratory is funded by the MRC [grant MC-US-A710]. Deposited in PMC for release after 6 months.

Competing interests statement

The authors declare no competing financial interests.

Supplementary material

Supplementary material available online at
http://dev.biologists.org/lookup/suppl/doi:10.1242/dev.080762/-/DC1

References

Abramoff, M. D., Magelhaes, P. J. and Ram, S. J. (2004). Image processing with Image J. *Biophotonics International* **11**, 36-42.
Baonza, A., Casci, T. and Freeman, M. (2001). A primary role for the epidermal growth factor receptor in ommatidial spacing in the Drosophila eye. *Curr. Biol.* **11**, 396-404.
Bertet, C., Sulak, L. and Lecuit, T. (2004). Myosin-dependent junction remodelling controls planar cell intercalation and axis elongation. *Nature* **429**, 667-671.
Blankenship, J. T., Backovic, S. T., Sanny, J. S., Weitz, O. and Zallen, J. A. (2006). Multicellular rosette formation links planar cell polarity to tissue morphogenesis. *Dev. Cell* **11**, 459-470.
Brodu, V. and Casanova, J. (2006). The RhoGAP crossveinless-c links trachealess and EGFR signaling to cell shape remodeling in Drosophila tracheal invagination. *Genes Dev.* **20**, 1817-1828.
Brown, K. E., Baonza, A. and Freeman, M. (2006). Epithelial cell adhesion in the developing Drosophila retina is regulated by Atonal and the EGF receptor pathway. *Dev Biol.* **300**, 710-721.
Chang, L. H., Chen, P., Lien, M. T., Ho, Y. H., Lin, C. M., Pan, Y. T., Wei, S. Y. and Hsu, J. C. (2011). Differential adhesion and actomyosin cable collaborate to drive Echinoid-mediated cell sorting. *Development* **138**, 3803-3812.
Chen, C. K. and Chien, C. T. (1999). Negative regulation of atonal in proneural cluster formation of Drosophila R8 photoreceptors. *Proc. Natl. Acad. Sci. USA* **96**, 5055-5060.
Classen, A. K., Anderson, K. I., Marois, E. and Eaton, S. (2005). Hexagonal packing of Drosophila wing epithelial cells by the planar cell polarity pathway. *Dev. Cell* **9**, 805-817.
Corrigall, D., Walther, R. F., Rodriguez, L., Fichelson, P. and Pichaud, F. (2007). Hedgehog signaling is a principal inducer of Myosin-II-driven cell ingression in Drosophila epithelia. *Dev. Cell* **13**, 730-742.
Dahmann, C. and Basler, K. (1999). Compartment boundaries: at the edge of development. *Trends Genet.* **15**, 320-326.

Dawes-Hoang, R. E., Parmar, K. M., Christiansen, A. E., Phelps, C. B., Brand, A. H. and Wieschaus, E. F. (2005). folded gastrulation, cell shape change and the control of myosin localization. *Development* **132**, 4165-4178.
Escudero, L. M., Bischoff, M. and Freeman, M. (2007). Myosin II regulates complex cellular arrangement and epithelial architecture in Drosophila. *Dev. Cell* **13**, 717-729.
Fernandez-Gonzalez, R., Simoes Sde, M., Roper, J. C., Eaton, S. and Zallen, J. A. (2009). Myosin II dynamics are regulated by tension in intercalating cells. *Dev. Cell* **17**, 736-743.
Irvine, K. D. and Wieschaus, E. (1994). Cell intercalation during Drosophila germband extension and its regulation by pair-rule segmentation genes. *Development* **120**, 827-841.
Jarman, A. P., Grell, E. H., Ackerman, L., Jan, L. Y. and Jan, Y. N. (1994). Atonal is the proneural gene for Drosophila photoreceptors. *Nature* **369**, 398-400.
Keller, R. (2002). Shaping the vertebrate body plan by polarized embryonic cell movements. *Science* **298**, 1950-1954.
Krahn, M. P., Klopfenstein, D. R., Fischer, N. and Wodarz, A. (2010). Membrane targeting of Bazooka/PAR-3 is mediated by direct binding to phosphoinositide lipids. *Curr. Biol.* **20**, 636-642.
Landsberg, K. P., Farhadifar, R., Ranft, J., Umetsu, D., Widmann, T. J., Bittig, T., Said, A., Julicher, F. and Dahmann, C. (2009). Increased cell bond tension governs cell sorting at the Drosophila anteroposterior compartment boundary. *Curr. Biol.* **19**, 1950-1955.
Le Borgne, R., Bellaiche, Y. and Schweisguth, F. (2002). Drosophila E-cadherin regulates the orientation of asymmetric cell division in the sensory organ lineage. *Curr. Biol.* **12**, 95-104.
Lee, A. and Treisman, J. E. (2004). Excessive Myosin activity in mbs mutants causes photoreceptor movement out of the Drosophila eye disc epithelium. *Mol. Biol. Cell* **15**, 3285-3295.
Levayer, R., Pelissier-Monier, A. and Lecuit, T. (2011). Spatial regulation of Dia and Myosin-II by RhoGEF2 controls initiation of E-cadherin endocytosis during epithelial morphogenesis. *Nat. Cell Biol.* **13**, 529-540.
Major, R. J. and Irvine, K. D. (2006). Localization and requirement for Myosin II at the dorsal-ventral compartment boundary of the Drosophila wing. *Dev. Dyn.* **235**, 3051-3058.
Martin, A. C., Kaschube, M. and Wieschaus, E. F. (2009). Pulsed contractions of an actin-myosin network drive apical constriction. *Nature* **457**, 495-499.
McKim, K. S., Dahmus, J. B. and Hawley, R. S. (1996). Cloning of the Drosophila melanogaster meiotic recombination gene mei-218: a genetic and molecular analysis of interval 15E. *Genetics* **144**, 215-228.
Monier, B., Pelissier-Monier, A., Brand, A. H. and Sanson, B. (2010). An actomyosin-based barrier inhibits cell mixing at compartmental boundaries in Drosophila embryos. *Nat. Cell Biol.* **12**, 60-65.
Neubueser, D. and Hipfner, D. R. (2010). Overlapping roles of Drosophila Drak and Rok kinases in epithelial tissue morphogenesis. *Mol. Biol. Cell* **21**, 2869-2879.
Nishimura, M., Inoue, Y. and Hayashi, S. (2007). A wave of EGFR signaling determines cell alignment and intercalation in the Drosophila tracheal placode. *Development* **134**, 4273-4282.
Oda, H. and Tsukita, S. (2001). Real-time imaging of cell-cell adherens junctions reveals that Drosophila mesoderm invagination begins with two phases of apical constriction of cells. *J. Cell Sci.* **114**, 493-501.
O'Keefe, D. D., Gonzalez-Nino, E., Burnett, M., Dylla, L., Lambeth, S. M., Licon, E., Amesoli, C., Edgar, B. A. and Curtiss, J. (2009). Rap1 maintains adhesion between cells to affect Egfr signaling and planar cell polarity in Drosophila. *Dev. Biol.* **333**, 143-160.
O'Neill, E. M., Rebay, I., Tjian, R. and Rubin, G. M. (1994). The activities of two Ets-related transcription factors required for Drosophila eye development are modulated by the Ras/MAPK pathway. *Cell* **78**, 137-147.
Peter, A., Schottler, P., Werner, M., Beinert, N., Dowe, G., Burkert, P., Mourkioti, F., Dentzer, L., He, Y., Deak, P. et al. (2002). Mapping and identification of essential gene functions on the X chromosome of Drosophila. *EMBO Rep.* **3**, 34-38.
Pilot, F. and Lecuit, T. (2005). Compartmentalized morphogenesis in epithelia: from cell to tissue shape. *Dev. Dyn.* **232**, 685-694.
Quintin, S., Gally, C. and Labouesse, M. (2008). Epithelial morphogenesis in embryos: asymmetries, motors and brakes. *Trends Genet.* **24**, 221-230.
Rauzi, M., Verant, P., Lecuit, T. and Lenne, P. F. (2008). Nature and anisotropy of cortical forces orienting Drosophila tissue morphogenesis. *Nat. Cell Biol.* **10**, 1401-1410.
Rauzi, M., Lenne, P. F. and Lecuit, T. (2010). Planar polarized actomyosin contractile flows control epithelial junction remodelling. *Nature* **468**, 1110-1114.
Ready, D. F., Hanson, T. E. and Benzer, S. (1976). Development of the Drosophila retina, a neurocrystalline lattice. *Dev. Biol.* **53**, 217-240.
Schlichting, K. and Dahmann, C. (2008). Hedgehog and Dpp signaling induce cadherin Cad86C expression in the morphogenetic furrow during Drosophila eye development. *Mech. Dev.* **125**, 712-728.
Scholz, H., Deatrick, J., Klaes, A. and Klambt, C. (1993). Genetic dissection of pointed, a Drosophila gene encoding two ETS-related proteins. *Genetics* **135**, 455-468.
Simoes Sde, M., Blankenship, J. T., Weitz, O., Farrell, D. L., Tamada, M., Fernandez-Gonzalez, R. and Zallen, J. A. (2010). Rho-kinase directs Bazooka/Par-3 planar polarity during Drosophila axis elongation. *Dev. Cell* **19**, 377-388.
Simone, R. P. and DiNardo, S. (2010). Actomyosin contractility and Discs large contribute to junctional conversion in guiding cell alignment within the Drosophila embryonic epithelium. *Development* **137**, 1385-1394.
Steinberg, M. S. (2007). Differential adhesion in morphogenesis: a modern view. *Curr. Opin. Genet. Dev.* **17**, 281-286.
Sweeton, D., Parks, S., Costa, M. and Wieschaus, E. (1991). Gastrulation in Drosophila: the formation of the ventral furrow and posterior midgut invaginations. *Development* **112**, 775-789.
Wallingford, J. B., Rowning, B. A., Vogeli, K. M., Rothbacher, U., Fraser, S. E. and Harland, R. M. (2000). Dishevelled controls cell polarity during Xenopus gastrulation. *Nature* **405**, 81-85.
Walters, J. W., Dilks, S. A. and DiNardo, S. (2006). Planar polarization of the denticle field in the Drosophila embryo: roles for Myosin II (zipper) and fringe. *Dev. Biol.* **297**, 323-339.
Wasserman, J. D., Urban, S. and Freeman, M. (2000). A family of rhomboid-like genes: Drosophila rhomboid-1 and roughoid/rhomboid-3 cooperate to activate EGF receptor signaling. *Genes Dev.* **14**, 1651-1663.
Wei, S. Y., Escudero, L. M., Yu, F., Chang, L. H., Chen, L. Y., Ho, Y. H., Lin, C. M., Chou, C. S., Chia, W., Modolell, J. et al. (2005). Echinoid is a component of adherens junctions that cooperates with DE-Cadherin to mediate cell adhesion. *Dev. Cell* **8**, 493-504.
Winter, C. G., Wang, B., Ballew, A., Royou, A., Karess, R., Axelrod, J. D. and Luo, L. (2001). Drosophila Rho-associated kinase (Drok) links Frizzled-mediated planar cell polarity signaling to the actin cytoskeleton. *Cell* **105**, 81-91.
Wodarz, A., Ramrath, A., Kuchinke, U. and Knust, E. (1999). Bazooka provides an apical cue for Inscuteable localization in Drosophila neuroblasts. *Nature* **402**, 544-547.
Wolff, T. and Ready, D. F. (1991). The beginning of pattern formation in the Drosophila compound eye: the morphogenetic furrow and the second mitotic wave. *Development* **113**, 841-850.
Zallen, J. A. and Wieschaus, E. (2004). Patterned gene expression directs bipolar planar polarity in Drosophila. *Dev. Cell* **6**, 343-355.
Zallen, J. A. and Blankenship, J. T. (2008). Multicellular dynamics during epithelial elongation. *Semin. Cell Dev. Biol.* **19**, 263-270.